Considerations in Estimating Horizontal Wind Gradients from an Individual Doppler Radar or a Network of Wind Profilers

STEVEN D. SMITH* AND ROBERT M. RABIN

NOAA Environmental Research Laboratories, National Severe Storms Laboratory, Norman, Oklahoma

(Manuscript received 14 December 1987, in final form 17 October 1988)

ABSTRACT

Applications of Doppler weather radar data to the analysis of wind fields are reviewed. Radial velocity measurements from a single radar are used to estimate horizontal wind vectors within small azimuthal sectors using two different models. One assumes a uniform wind, the other a linear wind within the sector. Errors in wind estimates owing to gradients of wind are derived using harmonic analysis. The radar data analysis techniques are tested on complex wind patterns which were reconstructed from dual-Doppler radar measurements.

1. Introduction

Recent plans for a Doppler radar network in the United States (NEXt generation weather RADar, or NEXRAD) is aimed at improving the detection of severe thunderstorms and tornadoes. These radars, however, will have sufficient sensitivity to provide Doppler wind measurements nearly continuously in the lower troposphere during all weather conditions, even in clear air. A planned network of UHF profiler radars in the Central United States will also provide Doppler measurements to greater altitudes. Unlike in situ measurements of wind, only the radial wind (components along the direction of the antenna) is estimated by the Doppler instrument; the net wind speed and direction is unknown without measurements by a second radar viewing from another angle. Radar separation in the NEXRAD and profiler networks will be too large to measure more than one component of the wind at the same point in space with multiple radars. Nonetheless, several other possibilities exist for using the observations. The most obvious is to input the measured radial wind components directly into the forecast model, leaving the undetected wind components to be supplied from other data sources. Moreover, if the complete three-dimensional wind field is desired for diagnostic purposes, it may be possible to obtain the undetected components from a forecast model and a series of observations of the radial wind field in time (Wolfsberg 1987). This approach is appealing; its feasibility remains to be demonstrated, however. Finally, one can estimate the other wind components by modeling the spatial variation of the wind in ad hoc ways, two of which will be examined in this paper.

Of the various models, the most common assume either that the wind is uniform over an area of data points (Lhermitte and Atlas 1961; Glover et al. 1968; Hogg et al. 1983) or that it changes linearly within a certain domain (Browning and Wexler 1968; Waldteufel and Corbin 1979; Koscielny et al. 1982). The uniform assumption is also used to estimate horizontal wind vectors from profiler radars. This is a consequence of the presence of only two nonvertical beams at each profiler site. The beams sample orthogonal wind components, but at different horizontal locations for a given height. Although the wind vector obtained from the uniform assumption is generally assumed to be quite accurate, this has never been rigorously confirmed. Small errors in the mean wind over each radar or profiler can cause major errors in computed gradients of the wind between adjacent sites.

The assumption of linear wind variation can be applied to data from NEXRAD-like radars with mechanically steerable antennae, since the beam can be positioned at considerably more than two positions at a given height. It has been recognized that the gradients inferred from the linear assumption contain errors due to nonlinear terms (Waldteufel and Corbin 1979); however, the effect of third- and higher-order terms have not been quantified.

The aim of this paper is to address several basic questions concerning the use of both the uniform and linear wind assumptions in determining wind vectors and gradients from single-Doppler data or a network of radars and profilers:

* Present affiliation: NEXRAD Group of Unisys Corporation, Trevose, Pennsylvania.

Corresponding author address: Dr. Robert M. Rabin, NOAA/National Severe Storms Laboratory, 1313 Halley Circle, Norman, OK 73069.

(i) How well is the mean wind estimated?

(ii) Can gradients of the wind be inferred by applying the uniform wind assumption over local volumes (above each profiler site, or within different subvolumes of single-Doppler radar data)?

(iii) Does the use of the linear assumption yield more reliable estimates of these gradients, or, should a more complex, non-linear wind model be used?

In order to answer these questions, techniques are first reviewed in section 2 which apply the uniform and linear wind assumptions to data on arcs of constant range from a radar. Then, random and systematic errors in the wind estimates from these techniques, and the implied errors in wind gradients, are examined in section 3. These errors are extended to a hypothetical network of profilers in section 4. A complex wind field derived from dual-Doppler analysis is used to test the errors associated with the uniform and linear wind models applied to single radar data in section 5. A summary and conclusions appear in section 6.

2. Techniques to infer wind vectors from single-Doppler data

a. Basic equations

The Cartesian components of the vector wind $\boldsymbol{U} = (u, v, w)$ are defined with u in the direction of x and positive eastward, v in the direction of y and positive northward, and w in the direction of z and positive upward. The wind components at arbitrary points (x_i, y_i, z_i), relative to the origin (x_0, y_0, z_0), are derived from the Taylor series expansions:

$$\boldsymbol{U}(x_i, y_i, z_i) = \boldsymbol{U}_0 + \frac{\partial \boldsymbol{U}}{\partial x}\Delta x + \frac{\partial \boldsymbol{U}}{\partial y}\Delta y + \frac{\partial \boldsymbol{U}}{\partial z}\Delta z + \text{higher-order terms}, \quad (1)$$

where, for example, $\boldsymbol{U}_0 = u(x_0, y_0, z_0)$ and $\Delta x = (x_i - x_0)$.

Radar sampling volume locations, at which measurements of Doppler velocity are made, are generally specified in reference to a local spherical coordinate system. These radar coordinates are slant range from the radar, r, radar beam elevation angle, θ, and azimuth angle measured clockwise from north, ϕ. For purposes of illustration and simplicity, we assume two-dimensionality so that Doppler measurements are strictly a projection of the horizontal wind. Furthermore, data locations are in reference to plane polar coordinates, with no elevation angle dependence. This will simplify the mathematical development greatly in sections to follow.

The Cartesian coordinates and plane polar coordinates of data points are functionally related by:

$$x = r\sin\phi$$
$$y = r\cos\phi. \quad (2)$$

With the aid of (2), expressions for the radial, v_r, and cross-beam, v_t, Doppler velocities in terms of (u, v) are

$$v_r = \boldsymbol{V}\cdot\boldsymbol{a}_r,$$
$$\boldsymbol{a}_r = (\boldsymbol{i}_x\sin\phi + \boldsymbol{i}_y\cos\phi);$$

and

$$v_t = \boldsymbol{V}\cdot\boldsymbol{a}_t,$$
$$\boldsymbol{a}_t = (\boldsymbol{i}_x\cos\phi - \boldsymbol{i}_y\sin\phi) \equiv \frac{\partial \boldsymbol{a}_r}{\partial\phi}, \quad (3)$$

where unit vectors $\boldsymbol{i}_x$ and $\boldsymbol{i}_y$ are in the directions of x and y, respectively. The unit vector in the direction of z, $\boldsymbol{i}_z$, does not appear because of the assumption of two-dimensionality.

Consider the radar "sampled" radial and the unobservable cross-beam velocities as discrete Fourier series in azimuth, periodic over a circle of measurement at constant range (this will facilitate examination of errors in wind vectors and gradients for any assumed spectra of velocities):

$$v_r(r, \phi_k) = \sum_{m=-M/2}^{M/2} S_m(r)\exp[j(m\phi_k)] \quad (4a)$$

$$v_t(r, \phi_k) = \sum_{m=-M/2}^{M/2} R_m(r)\exp[j(m\phi_k)], \quad (4b)$$

where $\phi_k = k\Delta$, Δ is the azimuthal spacing of samples in radians, k is an index defined from $-M/2$ to $M/2$, m is circular wavenumber or harmonic, $j = \sqrt{-1}$, and $M/2$ is the highest resolvable harmonic for data spaced by Δ. The range-dependent complex Fourier amplitudes, $S_m(r) = A_m(r) - jB_m(r)$ and $R_m(r) = C_m(r) - jD_m(r)$ are composed of real and imaginary parts corresponding to the cosine and sine amplitudes, respectively.

In section 2c, we relate the Fourier amplitudes of the radial and cross-beam components to kinematic properties of the Cartesian wind components. In the section 2b we specify the general form of the models used to specify the two-dimensional wind and the techniques used to solve for the model parameters.

b. Multivariate regression techniques

The first step of our single-Doppler wind analysis is to assume a model for the two-dimensional Cartesian wind. Relating the modeled Cartesian wind to the Doppler radial velocity:

$$v_r = \boldsymbol{P}_l\boldsymbol{K}_l^{\mathrm{T}} + \epsilon, \quad (5)$$

where v_r is the radial velocity, $\boldsymbol{K}_l$ is a vector of model parameters containing the kinematic properties of the Cartesian wind components, $\boldsymbol{P}_l$ is a vector of regressors, ϵ is that part of the observation unexplained by the

model, and T is the vector transpose. For N measurements of radial velocity within some as of yet unspecified analysis domain, the vector of velocity measurements V_N, is expressed as a matrix equation

$$V_N = P_{Nl}K_l^{\mathrm{T}} + \epsilon_N, \tag{6}$$

where ϵ_N is a $(N \times 1)$ vector of errors. The analysis domain could be a circular arc or a sector. A circular arc is a set of measurements over some azimuthal extent at constant range. A sector has both azimuthal and range extent.

The parameters of the model (6) are estimated using multivariate regression techniques. The least-squares solution for the estimated model parameters $\hat{K}_l$ is (Draper and Smith 1983)

$$\hat{K}_l = (P_{Nl}^{\mathrm{T}}P_{Nl})^{-1}P_{Nl}^{\mathrm{T}}V_N. \tag{7}$$

It can be shown that the set of l equations (7) is equivalent to the convolution of v_r and an l-dimensional weighting function h_l corresponding to the l-dimensions of $\hat{K}_l$

$$\hat{K}_i = \sum_{k=1}^{N} v_r(k)h_{iN}(k - k_0), \tag{8}$$

where $\hat{K}_i$ is element i of the vector $\hat{K}_l$ and k_0 corresponds to the location (r_0, ϕ_0).

The convolution theorem allows one to view these weighted sums as summations of scaled Fourier amplitudes. For data processed over circular arcs, the general relationship between the Fourier spectrum of Doppler velocity measurements over a circle (4a) and the least-squares estimates of model parameters (8) is

$$\hat{K}_i = \sum_{m=-M/2}^{M/2} S_m(r)H_i(m)\exp(jmk_0\Delta), \tag{9}$$

where H_i is element i of the vector H_l. The H_l is the set of Fourier transforms $H_1, H_2, \ldots, H_l$ of the weighting functions $h_1, h_2, \ldots, h_l$.

c. Data analysis on an arc: uniform wind model

Substituting the zero-order terms from (2) into (4), the projection of a uniform horizontal wind in the radial direction is

$$\begin{aligned} v_r &= (iu_0 + ju_0)\cdot a_r \\ &= S_1\exp(j\phi) + S_1^*\exp(-j\phi). \end{aligned} \tag{10a}$$

Equation (10a) relates a uniform wind to a fundamental harmonic variation of Doppler velocity in azimuth. The unobservable transverse wind varies sinusoidally in azimuth as well. The azimuthal derivative of (10a) reveals

$$\begin{aligned} \frac{\partial v_r}{\partial \phi} &= (iu_0 + jv_0)\cdot a_t \\ &= jS_1\exp(j\phi) - jS_1^*\exp(-j\phi) \\ &= R_1\exp(j\phi) + R_1^*\exp(-j\phi) \\ &\equiv v_t, \end{aligned} \tag{10b}$$

from which it follows directly that $R_1 = jS_1$. Hence, $A_1 = -D_1$ and $B_1 = C_1$. The relationship expressed by (10b) forms the basis of an algorithm known as the Sectorized Uniform Wind (SUW) algorithm currently being tested by NEXRAD (Smith 1986), and is also known as the dual beam method (Glover 1968).

For simplicity, we assume this uniform wind is sampled at constant range r_0 over an azimuthal arc of length $\Delta\phi$, centered at azimuth ϕ_0. Furthermore, to facilitate subsequent analysis, field points are defined relative to a rotated Cartesian coordinate system. This coordinate system is identical to the (x, y) system defined previously, with the exception that the axes are rotated clockwise through an angle ϕ_0 (Fig. 1a).

Allowing for measurement error and/or deviations from a uniform wind in (10), ϵ, the model relating the vector wind and radial velocity measurements is:

$$v_r(k) = (u_0'\sin\phi_k' + v_0'\cos\phi_k') + \epsilon_k, \tag{11}$$

where

$$u_0' = u_0\cos\phi_0 - v_0\sin\phi_0, \tag{12a}$$

$$v_0' = u_0\sin\phi_0 + v_0\cos\phi_0. \tag{12b}$$

Here, $k_0\Delta = \phi_0$ and $\phi_i' = (k_i - k_0)\Delta$; i.e., the ϕ_i' are angles relative to ϕ_0. By definition, u_0' is the cross-beam component at ϕ_0 and positive is in the direction of increasing ϕ. The other component, v_0', is directed along the beam at ϕ_0 and is positive for motions away from the radar. Hence, $v_t(r_0, \phi_0) = u_0'$, and $v_r(r_0, \phi_0) = v_0'$ (Fig. 1b).

Analytical expressions for the estimates of the horizontal wind components $(\hat{u}_0', \hat{v}_0')$ are derived in appendix A for radial velocity data equally spaced over an analysis arc.

d. Linear wind analysis within sectors

Next we include in our model constant horizontal variations of the Cartesian wind components over some processing area. The kinematic properties of this linear wind are assumed constant over the data acquisition period. These assumptions are those commonly used in the analysis of the velocity azimuth display (VAD) technique of Waldteufel and Corbin (1979).

For a linear wind field, the amplitudes of the zeroth, fundamental, and second harmonics of the radial wind over a circle about the radar (i.e., harmonic numbers $m = 0, 1, 2$) are proportional to the basic properties: divergence, translation, and deformation (Browning and Wexler 1968). Using (1) and (3),

$$\begin{aligned} v_r(r, \phi) = u_0\sin\phi + v_0\cos\phi &+ \frac{r}{2}\left(\frac{\partial u}{\partial x} + \frac{\partial v}{\partial y}\right) \\ &+ \frac{r}{2}\left(\frac{\partial v}{\partial x} + \frac{\partial u}{\partial y}\right)\sin 2\phi + \frac{r}{2}\left(\frac{\partial v}{\partial y} - \frac{\partial u}{\partial x}\right)\cos 2\phi, \end{aligned}$$

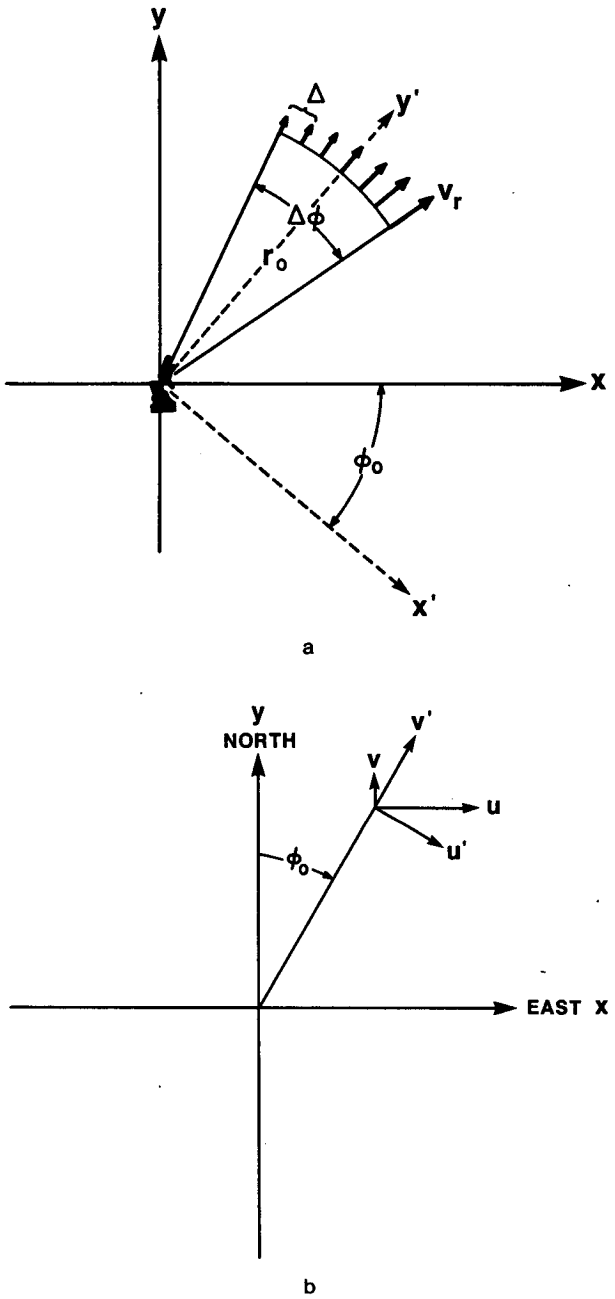

FIG. 1. (a) Geometry of the coordinate systems used in analyses. (b) Relationship between Cartesian wind components (u, v) and (u', v').

$$v_t(r, \phi) = u_0 \cos\phi - v_0 \sin\phi - \frac{r}{2}\left(\frac{\partial v}{\partial x} - \frac{\partial u}{\partial y}\right) + \frac{r}{2}\left(\frac{\partial v}{\partial x} + \frac{\partial u}{\partial y}\right)\cos 2\phi + \frac{r}{2}\left(\frac{\partial u}{\partial x} - \frac{\partial v}{\partial y}\right)\sin 2\phi, \quad (13)$$

where the origin is defined at the radar (i.e., $r_0 = 0$). It follows that $S_m(r) = -jR_m(r)$ for $m = \pm 1, \pm 2$ and $\partial S_m/\partial r = S_m/r \equiv -j\partial R_m/\partial r$ for $m \pm 2$. Furthermore, $R_0(r)$ and $S_0(r)$ are linear functions of range. All other Fourier coefficients are zero. The radial and cross-beam components specified in rotated coordinates (x', y') are found by replacing ϕ with ϕ' in (13). Consequently, all wind field parameters are relative to these rotated coordinates.

When the wind is uniform, measurements of v_r are sufficient to determine v_t [see (10)], whereas this is not the case when the wind is linear. As made apparent by (13), the mean vorticity about the radar is undetected. Therefore, the two-dimensional wind can not be retrieved from v_r measurements exclusively unless the flow is in the mean irrotational.

Least-squares solutions of the linear wind model parameters are presented in appendix B.

3. Random and systematic errors in the least-squares estimates of wind

Assessments of the utility of single-Doppler techniques designed to retrieve the mean wind can be made after evaluating some statistical properties of the estimators $\hat{u}_0'$, $\hat{v}_0'$ of the parameters u_0', v_0'. Two such properties are bias and variance. Variance measures the spread of the probability density function (PDF) of each estimator about its expected value due to random errors in measurements of radial velocity. On the other hand, bias is the amount by which the expected value of an estimator differs from the parameter it is estimating. This is a systematic departure and results from inadequacies of a model in replicating the true wind variations. Variance and bias are functions of analysis region geometry (Draper and Smith 1981) although dependencies on this geometry are quite different. In addition, biases depend on the true wind and are therefore difficult to quantify. Variance is proportional to velocity measurement uncertainty. In turn, measurement uncertainty is a function of radar system parameters (e.g., dwell time) and meteorological factors such as weather signal to noise power ratios and velocity spectrum width (Doviak and Zrnić, 1984). Quantitative estimates of measurement uncertainty are possible, so analysis region geometry can be designed to minimize its effect on estimate variance.

The main thrust of this paper is not a complete analysis of variance because the variance associated with least-squares estimates of wind field parameters has been thoroughly documented (Doviak and Zrnić, 1984; Koscielny, Doviak, and Zrnić 1984; Smith 1986). Nevertheless, the question of the validity of wind estimates needs to be answered. This differs from the more traditional approach to least-squares where observations are fit to an assumed model and the "goodness of fit" determines the model adequacy. It will become obvious that a model which fits observations perfectly does not necessarily imply model adequacy.

Typically, horizontal wind estimates are biased, whether they are derived from v_r measurements by as-

suming uniformity, linearity, or any other reasonable functional form of the Cartesian wind components over some processing area. Quantifying biases in wind estimates is the subject of the following sections.

a. *Errors in uniform wind estimates due to constant gradients of wind*

For a linear wind, we know that the complex amplitudes of the radial and transverse winds are defined at harmonic numbers $m = 0, \pm 1, \pm 2$ and zero otherwise. For data processed over circular arcs, the bias equations for the uniform wind estimates derived with the aid of (13) are:

$$\text{BIAS}[\hat{u}_0'] = \frac{r_0}{2}[(|H_1(2)| - 1)|\text{DEF}| \times \sin 2(\phi_0 - \phi_D) - \text{VOR}] \quad (14a)$$

$$\text{BIAS}[\hat{v}_0'] = \frac{r_0}{2}[(|H_2(0)| - 1)\text{DIV} + (|H_2(2)| - 1)|\text{DEF}| \cos 2(\phi_0 - \phi_D)], \quad (14b)$$

where H_1 and H_2 are Fourier transforms of weight functions, given in appendix A. The abbreviation VOR denotes the vertical vorticity, $-2C_0/r$, DIV denotes horizontal divergence, $2A_0/r$, and |DEF| denotes the magnitude of the horizontal deformation, $4/r[(A_2)^2 + (B_2)^2]^{1/2}$. The angle ϕ_D is defined by

$$\phi_D = -\frac{1}{2}\tan^{-1}\left(\frac{B_2}{A_2}\right),$$

and that angle is subtended by the deformation axis of dilatation and the north–south y-axis, measured clockwise from north.

Three examples were chosen to illustrate the uniform wind analysis and the biases in (14). Table 1 indicates the true spatial variations of the Cartesian wind components assumed in each example. The constant C_1 in the table is arbitrary. These three wind fields are depicted graphically in Fig. 2a–c. They are related, since the wind field in Example 3 produces the wind field illustrated in Example 1 by adding positive vorticity of magnitude $C_1/2$, whereas it produces the wind field in Example 2 by adding vorticity of the opposite sign.

The biases, although not derived explicitly for each example, are the vector differences between the true and resultant winds at each point. Obviously, these biases differ in each example. By projecting the true winds in each example onto radar radials, however, it can be shown that the Doppler-observed wind fields are identical. Thus, more importantly than the biases, the derived winds from the single Doppler analyses must be the same (Fig. 3).

TABLE 1. Three simulated wind fields.

	Example number		
	1	2	3
u	0	$C_1 y$	$C_1 y/2$
v	$C_1 x$	0	$C_1 x/2$

Kinematic properties of the wind such as horizontal divergence, vertical vorticity, and horizontal deformation are not explicitly estimated, but can be calculated from the uniform wind analysis results. This is done by taking horizontal derivatives of the least-squares estimates of the wind. To facilitate the interpretation of the biases in estimates of these kinematic properties, we again assume a linear wind. The bias equations are:

$$\text{BIAS}[\widehat{\text{DIV}}] = \text{DIV}[|H_2(0)| - 1] + |\text{DEF}|[|H_2(2)| - |H_1(2)|]\sin 2(\phi_0 + \phi_D),$$

$$\text{BIAS}[\widehat{\text{DEF}}_{\text{str}}] = -|\text{DEF}|[|H_2(2)| - 1] \times \cos 2(\phi_0 - \phi_D)\sin 2\phi_0 - |\text{DEF}|[|H_1(2)| + 1] \times \sin 2(\phi_0 - \phi_D)\cos 2\phi_0,$$

$$\text{BIAS}[\widehat{\text{DEF}}_{\text{shr}}] = |\text{DEF}|[|H_2(2)| - 1]\cos 2\phi_0 \times \cos 2(\phi_0 - \phi_D) + |\text{DEF}|[|H_1(2)| + 1] \times \sin 2\phi_0 \sin 2(\phi_0 - \phi_D),$$

$$\text{BIAS}[\widehat{\text{VOR}}] = |\text{DEF}|[|H_2(2)| - |H_1(2)| - 2] \times \cos 2(\phi_0 - \phi_D) - \text{VOR}. \quad (15)$$

The biases in $\widehat{\text{VOR}}$, $\widehat{\text{DIV}}$, and $|\widehat{\text{DEF}}|$, scaled by |DEF|, are illustrated in Fig. 4a as a function of viewing angle from the deformation axis of dilatation ϕ_D. The bias in $\hat{\phi}_D$ as a function of viewing angle is shown graphically in Fig. 4b. For convenience, we have assumed the divergence, vorticity, and magnitude of deformation were equal, and arbitrarily chose $\Delta\phi$ to be 30°.

Although there is substantial variation of the estimated divergence in azimuth, the mean divergence over a circle is (approximately) unbiased. Not surprisingly, the estimate of vorticity is biased in the mean by the true vorticity. As expected, the analysis of single-Doppler radar data filters the large-scale vorticity such that the resultant wind field is irrotational in the mean. The estimate of the magnitude of the deformation is in the mean overestimated (in this example by approximately |DEF|/2), whereas the estimate of the deformation axis of dilatation is unbiased in the mean.

b. *Errors in uniform wind estimates due to nonlinearities*

The derivation of analytic expressions for biases owing to higher order wind derivatives can be very tedious. Also, there is no upper bound to the order needed. A natural starting point would be second-order terms.

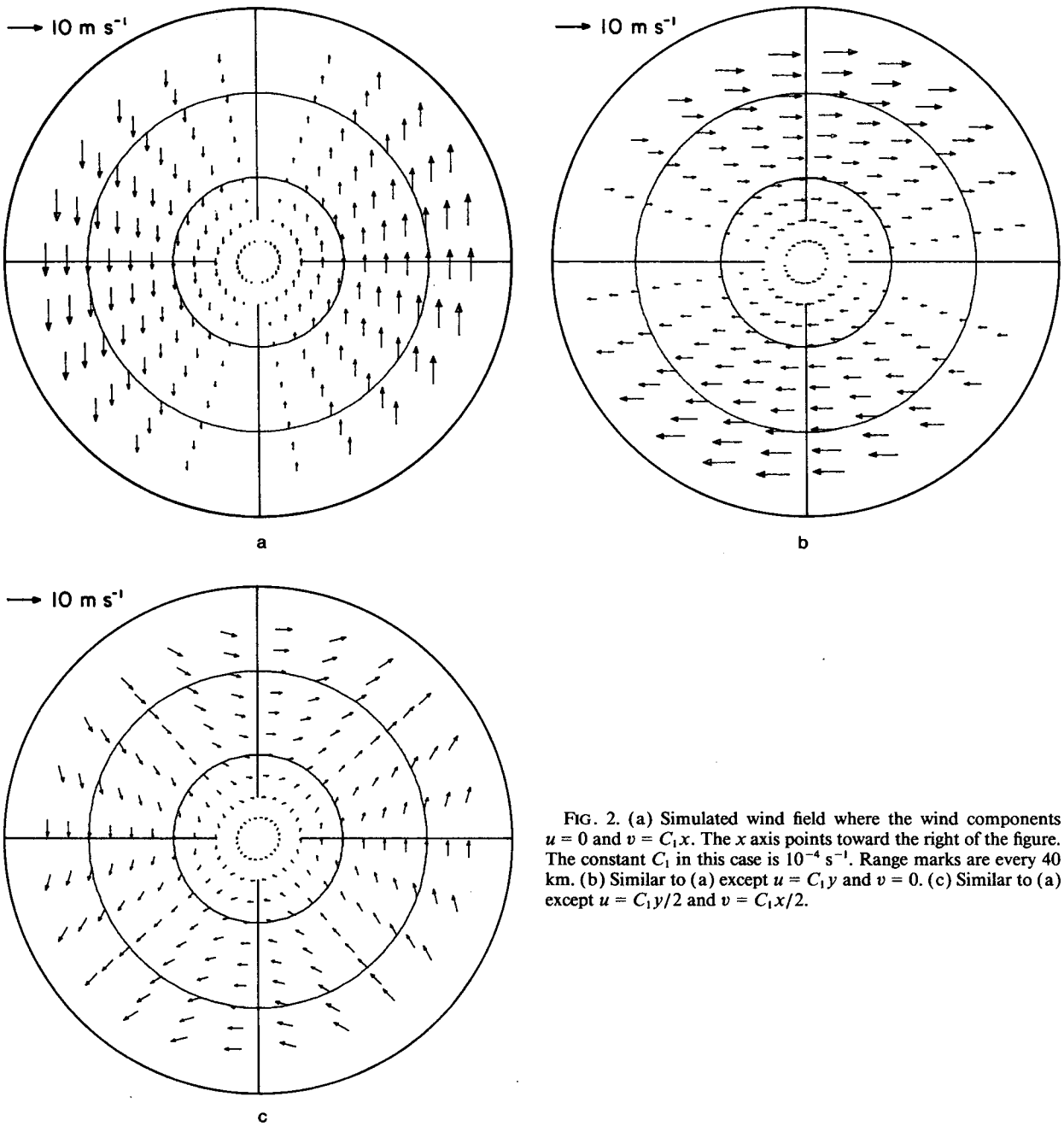

FIG. 2. (a) Simulated wind field where the wind components $u = 0$ and $v = C_1 x$. The x axis points toward the right of the figure. The constant C_1 in this case is 10^{-4} s^{-1}. Range marks are every 40 km. (b) Similar to (a) except $u = C_1 y$ and $v = 0$. (c) Similar to (a) except $u = C_1 y/2$ and $v = C_1 x/2$.

Considering all first- and second-order horizontal derivatives of the wind, the relationship between the vector wind and the radial velocity is

$$v_r(r, \phi) = \left\{u_0 + \frac{r^2}{8}\left[3\frac{\partial}{\partial x}(\mathrm{DIV}) - \frac{\partial}{\partial y}(\mathrm{VOR})\right]\right\} \times \sin\phi + \left\{v_0 + \frac{r^2}{8}\left[3\frac{\partial}{\partial y}(\mathrm{DIV}) + \frac{\partial}{\partial x}(\mathrm{VOR})\right]\right\} \times \cos\phi + \frac{r}{2}[\mathrm{DIV}] + \frac{r}{2}[\mathrm{DEF_{str}}]\cos 2\phi + \frac{r}{2}[\mathrm{DEF_{shr}}]\sin 2\phi - \frac{r^2}{8}\left[\frac{\partial}{\partial y}(\mathrm{DEF_{shr}}) + \frac{\partial}{\partial x}(\mathrm{DEF_{shr}})\right]\cos 3\phi + \frac{r^2}{8}\left[\frac{\partial}{\partial y}(\mathrm{DEF_{shr}}) - \frac{\partial}{\partial x}(\mathrm{DEF_{str}})\right]\sin 3\phi. \quad (16)$$

The components of the resultant deformation |DEF| are the shearing deformation, $\mathrm{DEF_{shr}}$, and the stretching deformation, $\mathrm{DEF_{str}}$. To illustrate biases in least-

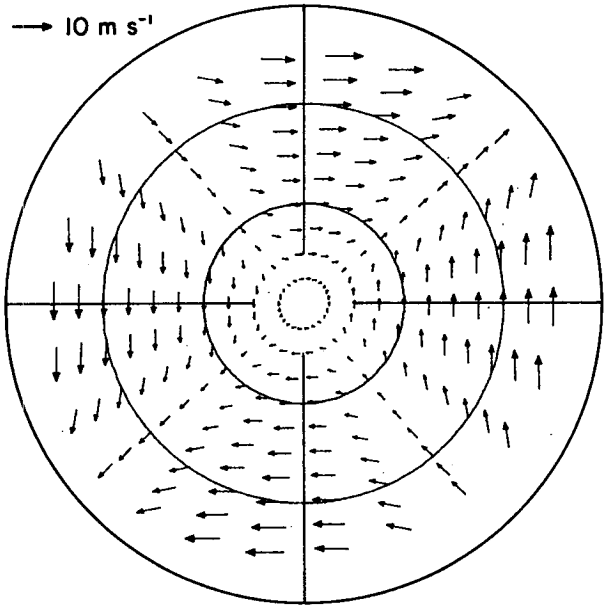

FIG. 3. Derived wind field from the radial components of the wind fields in Fig. 2a–c. The assumption of uniform, horizontal Cartesian wind components was made.

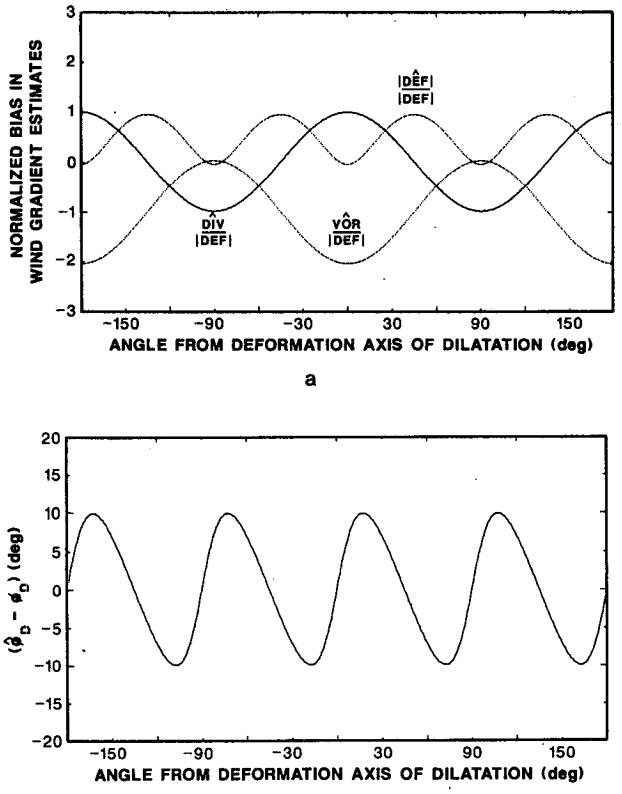

FIG. 4. (a) Biases in $\widehat{\text{VOR}}$, $\widehat{\text{DIV}}$, and $\widehat{|\text{DEF}|}$, scaled by |DEF|, as a function of viewing angle from the deformation axis of dilatation ϕ_D. (b) The bias in $\hat{\phi}_D$ as a function of viewing angle from the deformation axis of dilatation.

squares estimates owing to second-order nonlinearities, we assume a wind field of the form

$$v = \frac{\partial^2 v}{\partial x^2}\frac{x^2}{2},$$
$$u = 0. \qquad (17)$$

(Fig. 5a). From (3), radial and transverse components of this simulated field are

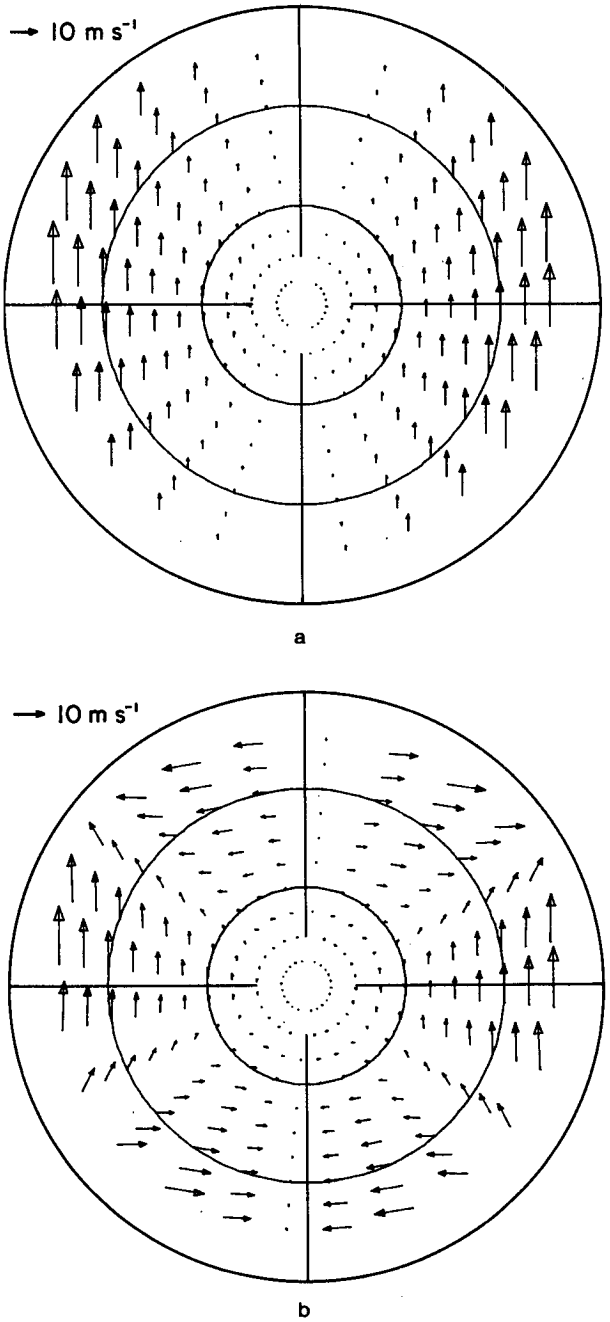

FIG. 5. Simulated wind field with $u = 0$ and $v = C_1x^2/2$. Here, $C_1 = 5 \times 10^{-9}$ m^{-1} s^{-1}. (b) Derived wind field from the radial wind components in (a) using the uniform wind model.

$$v_r(r, \phi) = \frac{\partial^2 v}{\partial x^2}\frac{r^2}{8}[\cos 3\phi - \cos\phi]$$

$$v_t(r, \phi) = \frac{\partial^2 v}{\partial x^2}\frac{r^2}{8}[\sin 3\phi - 3\sin\phi]. \quad (18)$$

The least-squares estimates of the radial and cross-beam wind components are derived from (9):

$$\hat{u}'_0(r_0, \phi_0) = \frac{\partial^2 v}{\partial x^2}\frac{r^2}{8}[|H_1(1)|\sin\phi_0 - |H_1(3)|\sin 3\phi_0],$$

$$\hat{v}'_0(r_0, \phi_0) = \frac{\partial^2 v}{\partial x^2}\frac{r^2}{8}[|H_2(3)|\cos 3\phi - |H_2(1)|\cos\phi_0]. \quad (19)$$

For radar data processed over 30° arcs, the resultant wind field is shown in Fig. 5b. Subtracting (18) from (19), the biases in wind estimates are

$$\text{BIAS}[\hat{u}'_0] = \frac{\partial^2 v}{\partial x^2}\frac{r^2}{8} \times [(|H_1(1)| - 3)\sin\phi_0 - (|H_1(3)| - 1)\sin 3\phi_0],$$

$$\text{BIAS}[\hat{v}'_0] = \frac{\partial^2 v}{\partial x^2}\frac{r^2}{8}[(|H_2(3)| - 1) \times \cos 3\phi_0 - (|H_2(1)| - 1)\cos\phi_0]. \quad (20)$$

For 30° arcs, the bracketed term in the expression for $\hat{u}'_0$ is on the order of 2 (appendix A), indicating that cross-beam wind estimates are severely biased. On the other hand, the bracketed term in the expression for $\hat{v}'_0$ is on the order of 0.1. Thus small biases appear in the radial wind estimates.

c. Systematic errors in linear wind estimates resulting from gradients of shear of the horizontal wind

We do not consider bias errors resulting from uniform gradients of the wind because the only wind field parameter of consequence is the vertical vorticity. As indicated by Eq. (14a), the bias in the transverse wind estimates is given by the product of one-half the vorticity and the center range of the analysis sector or arc. Otherwise, mean wind estimates are unaffected by uniform gradients of the wind.

Second-order wind variations bias linear wind estimates just as was the case for uniform wind estimates. Quantitative evaluation of the bias is difficult without knowing the scaling functions which multiply the Fourier amplitudes. However, the scaling functions for a linear wind analysis over a circle are known (appendix B). Assuming a wind field given by (17), the biases in the mean wind estimates are

$$\text{BIAS}[\hat{u}_0] = \frac{r^2}{8}\left[3\frac{\partial}{\partial x}(\text{DIV}) - \frac{\partial}{\partial y}(\text{VOR})\right],$$

$$\text{BIAS}[\hat{v}_0] = \frac{r^2}{8}\left[3\frac{\partial}{\partial y}(\text{DIV}) + \frac{\partial}{\partial x}(\text{VOR})\right]. \quad (21)$$

This result is extremely interesting because biases in the VAD derived estimates of wind traditionally have been ignored. According to Waldteufel and Corbin (1979), a typical order of magnitude of the mesoscale wind parameters appearing in (21) is 5×10^{-9} m^{-1} s^{-1}. At a range of 100 km, the bias in mean wind estimates can be as large as 6 m s^{-1}.

4. Errors in wind gradients using a network of profilers

Profilers measure the radial velocity along at least two beams tilted from the vertical. The processing of profiler data presumes local wind uniformity as follows (Strauch et al. 1984; Hogg et al. 1983). If a vertical beam is available, vertical winds measured at each height, h, overhead are assumed to be the same at the location of the other beams, which actually are displaced horizontally by an amount d:

$$d = h\cot\theta, \quad (22)$$

where θ is the elevation angle of the nonvertical beams. The vertical wind is then used to solve for the orthogonal, horizontal wind components at the location of the nonvertical beams. Finally, it is assumed that these horizontal wind components are valid at the same height above the radar. Assuming this methodology for processing profiler data, the bias errors in the horizontal wind owing to constant gradients of wind are given by (Koscielny et al. 1984):

$$\text{BIAS}\begin{bmatrix}\hat{u}_0\\ \hat{v}_0\end{bmatrix} = h\begin{bmatrix}\dfrac{\partial u}{\partial x}\cot\theta + \dfrac{\partial w}{\partial x}\\ \dfrac{\partial v}{\partial y}\cot\theta + \dfrac{\partial w}{\partial y}\end{bmatrix}. \quad (23)$$

Thus, errors in wind estimates at a given height are affected inversely by the elevation angle (instrument dependent) and directly by local wind gradients. The latter are spatially and temporally variable. If wind gradients are to be determined from wind estimates at adjacent profiler sites, the errors owing to the local wind gradients in (23) must be accounted for.

Consider a network of profilers separated in x and y by δx and δy. Horizontal gradients estimated between adjacent profilers will be substantially in error if the true horizontal gradients of u, v, and w vary significantly over δx and δy. For example, the bias errors in computing the components of the local divergence is given by:

$$\text{BIAS}\begin{bmatrix}\dfrac{\partial \hat{u}}{\partial x}\\ \dfrac{\partial \hat{v}}{\partial y}\end{bmatrix} = h\begin{bmatrix}\dfrac{\partial^2 u}{\partial x^2}\cot\theta + \dfrac{\partial^3 u}{\partial x^3}h + \dfrac{\partial^3 v}{\partial y \partial x^2}h\\ \dfrac{\partial^2 v}{\partial y^2}\cot\theta + \dfrac{\partial^3 u}{\partial y \partial x^2}h + \dfrac{\partial^3 v}{\partial y^3}h\end{bmatrix}, \quad (24)$$

when the horizontal divergence is constant with height and incompressibility is assumed.

In order to infer the bias from (24), let us consider a pattern of divergence which is horizontally symmetric about the point (x_0, y_0) given by sinusoidal variations in u and v:

$$u = A \sin\left[\frac{2\pi k}{L}(x - x_0)\right], \tag{25a}$$

$$v = A \sin\left[\frac{2\pi k}{L}(y - y_0)\right], \tag{25b}$$

$$\frac{\partial u}{\partial x} = \frac{2\pi k}{L} A \cos\left[\frac{2\pi k}{L}(x - x_0)\right], \tag{25c}$$

$$\frac{\partial v}{\partial y} = \frac{2\pi k}{L} A \cos\left[\frac{2\pi k}{L}(y - y_0)\right], \tag{25d}$$

where A is some constant amplitude, k is a nondimensional wave number, and L is the fundamental wavelength. The biases can be written as fractions of the true gradients:

$$\text{BIAS}\begin{bmatrix} \dfrac{\partial \hat{u}}{\partial x} \Big/ \dfrac{\partial u}{\partial x} \\ \dfrac{\partial \hat{v}}{\partial y} \Big/ \dfrac{\partial v}{\partial y} \end{bmatrix} = h\begin{bmatrix} \dfrac{2\pi k}{L}\tan\left[\dfrac{2\pi k}{L}(x - x_0)\right]\cot\theta - h\left[\dfrac{2\pi k}{L}\right]^2 \\ \dfrac{2\pi k}{L}\tan\left[\dfrac{2\pi k}{L}(y - y_0)\right]\cot\theta - h\left[\dfrac{2\pi k}{L}\right]^2 \end{bmatrix}. \tag{26}$$

Now velocity perturbations, of horizontal size larger than the station separation, are sufficiently sampled in space and time. The smallest wavelength (L/k) resolvable by the spaced profilers is $2\delta x$ and $2\delta y$ in the x and y directions, respectively. Assuming typical propagation speeds, c, atmospheric disturbances require time t, $(\Delta x/c, \Delta y/c)$, to traverse the distance between observation stations. Observations more frequent than $1/t$ cannot be adequately used. Assuming that wind soundings are filtered and sampled at $1/t$ to remove aliasing of waves smaller than L/k, then L/k should be replaced by $2\delta x$, $2\delta y$ in (26) and the biases are inversely proportional to the station spacing. At heights near 5 km and for typical elevation angles ($\approx 75°$) and spacing of 100 km, the greatest magnitude of the biases in (26) are about 0.06, or 6%. However, with more closely spaced profilers, the error becomes substantial: 42% for example when the profilers are only 10 km apart. Hence, the spacing appears quite critical. Unfortunately, the high temporal resolution afforded by profilers cannot be utilized fully without close spacing, since temporal filtering is required to reduce aliasing of smaller scale waves. For example, it takes up to 3 h for waves not fully resolved by a network with spacing of 100 km to be averaged out from a particular profiler record if the wave speed is 30 km h^{-1}.

5. Evaluation of wind estimate errors from single-Doppler data using a complex wind field

Natural wind fields are found to contain a continuous spectrum of eddies with different size and intensity (Doviak and Berger 1980). Such fields are composed of a multitude of higher-order horizontal derivatives. Rather than devising an analytic expression for a natural wind field, actual winds derived from a dual-Doppler radar analysis were chosen to test the uniform and linear wind models. The data were collected during early convective development on 17 May 1981 using the two 10-cm radars of the National Severe Storms Laboratory (NSSL). The dual radar synthesized wind field covers an area 60×80 km^2 at a constant altitude of 0.75 km. Fig. 6a is the dual-Doppler derived wind field resampled in (r, ϕ) coordinates, assuming a hypothetical radar located in the middle of the analysis plane. In order to illustrate the deviation from a uniform wind, a mean wind (12 m s^{-1} at 220°) has been subtracted from the field in Fig. 6a.

The uniform wind and linear wind models were applied to radial wind data derived from the perturbations plus mean wind in Fig. 6a. The derived perturbations and mean winds from both models are shown for comparison on Fig. 6b–d. The wind vectors shown in Fig. 6b were obtained from the uniform wind model using data along 30° arcs (30 points) at constant range, while those in Fig. 6c from data within sectors of azimuth width $\Delta\phi = 40°$ and range width $\Delta r = 10$ km. The wind vectors in 6d at constant range were constructed from a linear wind analysis along a circle at the same range (i.e., analysis of the VAD) using a truncated Taylor series expansion to derive the wind components u, v at field points, i.e.:

$$\hat{u}(r_0, \phi) = \hat{u}_0(r = 0) + \frac{1}{2}\widehat{\text{DIV}} r_0 \sin\phi + \frac{1}{2}\widehat{\text{DEF}_{\text{str}}} r_0 \sin\phi + \frac{1}{2}\widehat{\text{DEF}_{\text{shr}}} r_0 \cos\phi,$$

$$\hat{v}(r_0, \phi) = \hat{v}_0(r = 0) + \frac{1}{2}\widehat{\text{DIV}} r_0 \cos\phi - \frac{1}{2}\widehat{\text{DEF}_{\text{str}}} r_0 \cos\phi + \frac{1}{2}\widehat{\text{DEF}_{\text{shr}}} r_0 \sin\phi, \tag{27}$$

where the range r_0 indicates the location of radial wind data.

Although the linear wind model applied uses more data and has effectively less resolution, the uniform wind analysis over arcs produces a much smoother field and generally compares better to the actual winds. We attribute this, in part, to the sectors being too small to estimate the mean wind as well as the gradient terms adequately. The smoothest wind field is the one produced from the VAD output.

For an x' axis orientated from the southwest through the northeast, there is a noticeable gradient, $\partial v'/\partial x' > 0$. Because the mean vorticity is undetected by a single Doppler radar, this gradient manifests itself as a

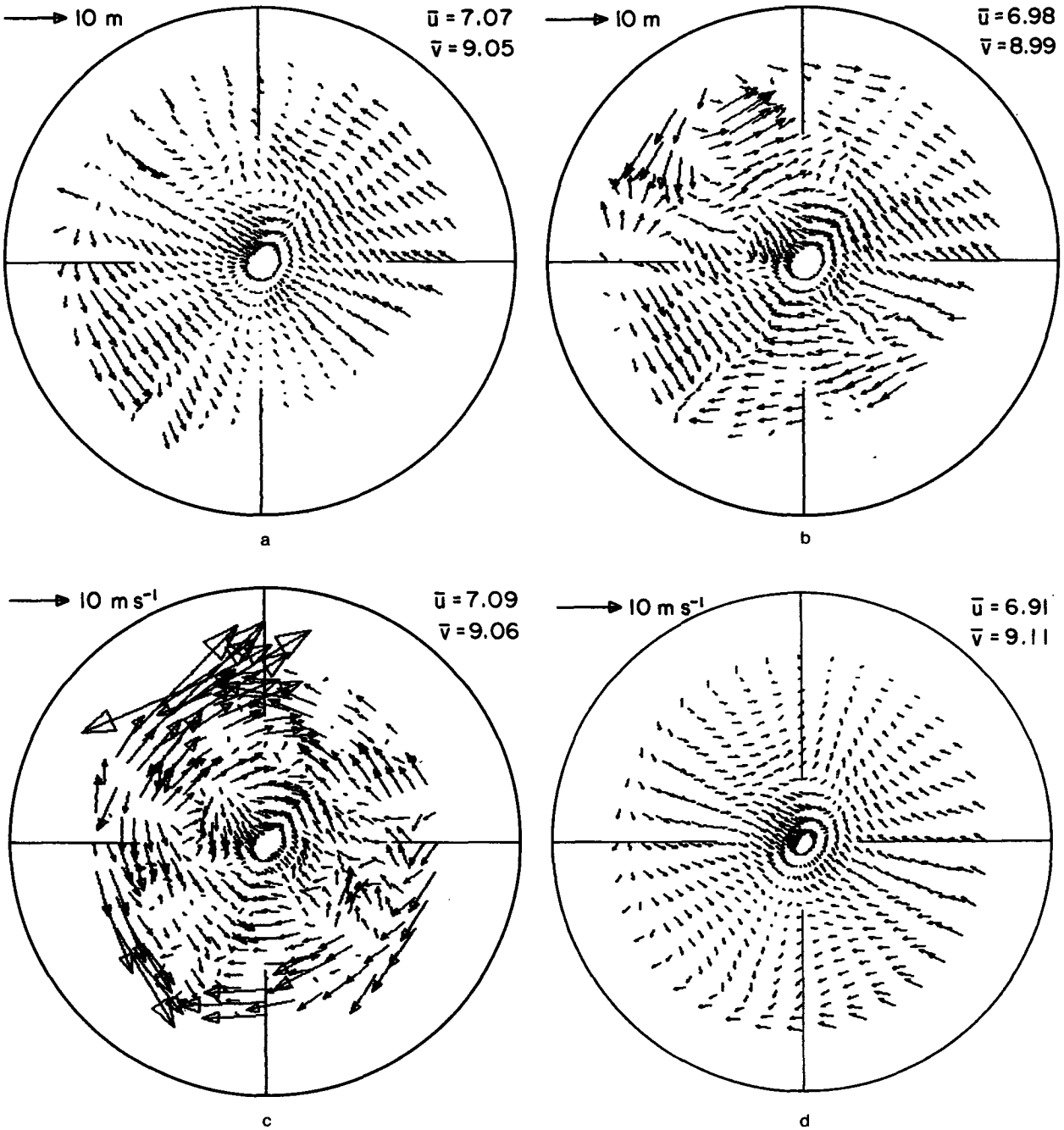

FIG. 6. (a) Perturbation wind field from dual-radar analysis on a horizontal surface. Mean wind components are shown in upper right corner of figure. The outer range ring is 40 km. (b) Results from the analysis of the wind field shown in (a) using the uniform wind model. Only the perturbation winds are shown. The mean wind components are shown in the upper right corner of the figure. (c) Same as in (b) except using the linear wind model. (d) Same as in (b) except reconstructed from output of the analysis of the VAD.

fictitious cross-beam wind gradient along the y' axis (southeast through northwest). This gradient is illustrated in Figs. 6b–6d. For this example, the most reliable wind estimates are along the x' axis.

Despite relatively large errors in individual wind vectors when applying the uniform and linear wind models, it is noteworthy that the areal averaged wind indicated in Fig. 6 varies by less than 0.2 m s^{-1} (2% of the total wind speed). It is difficult to generalize this result, however; the error in individual wind vectors, and hence local derivatives, appear to be far more serious than error in the average wind.

6. Discussion and conclusions

The estimation of horizontal wind vectors from single-Doppler radar data has been examined for methods which assume local uniform and linear wind variation of the Cartesian wind components. Both methods suffer from the fact that single radar data does not contain information on the mean vertical vorticity. In addition, output wind vectors from each model are biased by spatial wind derivatives which are higher order than assumed in each model. Therefore, local wind derivatives tend to be biased, limiting quantitative use of such techniques. For example, this was shown to be the case when applying the uniform wind assumption to a linear wind field. The biases in wind derivative estimates at points were found to be on the same order of magnitude as the true wind derivatives. Hence, in general, gradients can not be inferred by applying the uniform wind assumption on local volumes. However, when averaged around a circle centered over the radar, the estimated divergence was (approximately) unbiased, whereas the resultant magnitude of deformation was overestimated by an amount which could be determined from the least-squares response functions.

The uniform wind assumption can be applied in certain situations with positive results. It has been applied to radar data within convective storms as a means to retrieve wind profiles (Zrnić et al. 1986). The results compared with rawinsonde and dual-Doppler-derived wind profiles show differences in wind vectors generally being less than 30° in wind direction and 10 m s^{-1} in wind speed. It has also been applied within sectors on either side of detected gust fronts to obtain estimates of the wind shift across the front (Witt and Smith 1987).

This paper has demonstrated how the accuracy of mean wind estimates depend on the linearity assumption, even for the VAD. Estimates are biased by higher-order wind derivatives as well as the mean vorticity. For data processed within sectors displaced from the radar, the bias owing to vorticity is given by the product of one-half the vorticity and the range to the processing sector. For data analyzed over a circle, mean wind estimates at the radar site are unaffected by vorticity but do depend on nonlinearities. The exact error in the areal mean wind estimate can not be generalized, since it depends on the form of the true wind field. However, using a dual-Doppler wind field as a test, the error in the areal average wind was much less than 2%, although the error in individual wind vectors was in general very substantial. We have shown that gradients of divergence and vorticity could bias mean winds by several m s^{-1}. In fact, errors in the wind vectors were shown to be at least as large when applying the linear wind model vs. the uniform wind model. Based on this observation, it is unclear whether results could be improved with more complex, nonlinear wind models.

Finally, the effect of the local uniform wind assumption in computing winds from a network of profilers was examined. (This assumption is invoked if each profiler is limited to two nonvertical beam positions.) The errors in gradients are generally negligible if the spacing is greater than 100 km. Closer spacing, although desirable to improve spatial sampling, can render significant errors in the computed horizontal wind gradients. The basis for this result is that the inclusion of shorter waves, inherent with reduced spacing, leads to increasing errors in horizontal derivatives. For a given set of nonequal wind errors at adjacent sites, the errors in the velocity gradients are inversely proportional to the distance between sites.

Acknowledgments. The authors would like to thank the Interim Operational Test Facility of NEXRAD for supporting this research. Joan Kimpel prepared some of the figures. Sandra McPherson patiently typed revisions to the manuscript. Special thanks go to Mr. Mike Eilts and Drs. Dusan Zrnić, Charles Doswell and Robert Maddox for their reviews.

APPENDIX A

Least-Squares Solution for Uniform Wind Model

Assuming a uniform wind, $l = 2$ parameters and the vectors $\boldsymbol{P}_{2_i}$ and $\boldsymbol{K}_2$, are defined as

$$\boldsymbol{P}_{2_i} = [\sin\phi_i' \quad \cos\phi_i'],$$

$$\boldsymbol{K}_2 = [u_0' \quad v_0'], \tag{A1}$$

so that least-squares estimates of $\boldsymbol{K}_2$ are

$$\hat{\boldsymbol{K}}_2 = (\boldsymbol{P}_2^{\mathrm{T}}\boldsymbol{P}_2)^{-1}\boldsymbol{P}_2^{\mathrm{T}}\boldsymbol{V}. \tag{A2}$$

Evaluating the matrix multiplications for N equally spaced measurements along a circular arc $\Delta\phi$:

$$\hat{u}_0'(k) = \sum v_r(i)h_1(i-k) \equiv \frac{\sum v_r(i)\sin[(i-k)\Delta]}{\sum \sin^2[(i-k)\Delta]},$$

$$\hat{v}_0'(k) = \sum v_r(i)h_2(i-k) \equiv \frac{\sum v_r(i)\cos[(i-k)\Delta]}{\sum \cos^2[(i-k)\Delta]}, \tag{A3}$$

where all summations are from $i = 1$ to N. A result similar to (A3) applies to data processed over sectors of range width Δr with the exception that $v_r(i)$ is replaced by its range-averaged (over Δr) value. Range-averaging has the advantage of reducing the uncertainty of horizontal wind estimates introduced by errors in radial velocity measurements.

The Fourier transforms of the weight functions h_1 and h_2 in (A3) are:

$$H_1(m) = \frac{-j}{2c_1}\{(\exp[j(n+1)(m+1)\Delta] - \exp[-jn(m+1)\Delta])/\exp[j(m+1)\Delta] + (\exp[jn(m-1)\Delta] - \exp[j(n+1)(m-1)\Delta])/\exp[j(m-1)\Delta]\}, \tag{A4a}$$

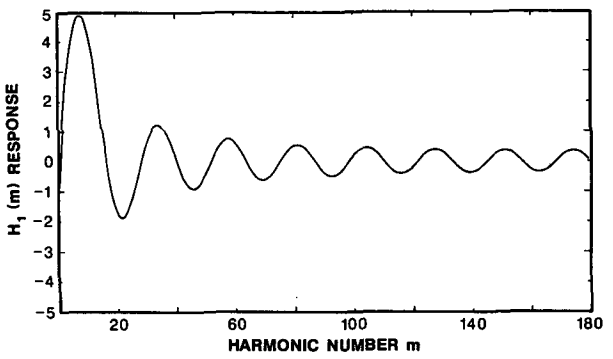

FIG. A1. Response function $H_1(m)$ as a function of harmonic number m for the cross-beam wind estimate. Sector size, $\Delta\phi$, is 30°.

and

$$H_2(m) = \frac{1}{2c_2}\{(\exp[j(n+1)(m+1)\Delta] - \exp[jn(m+1)\Delta])/\exp[j(m+1)\Delta] + (\exp[j(n+1)(m-1)\Delta] - \exp[jn(m-1)\Delta])/\exp[j(m-1)\Delta]\}. \quad \text{(A4b)}$$

It can be shown that H_2 is a real-valued function and H_1 is complex so that the following relationships hold:

$$H_1 = j|H_1|,$$
$$H_2 = |H_2|, \quad \text{(A5)}$$

where the brackets denote magnitude. The constants c_1 and c_2 in (A4) are defined by the denominators of (A3), and $n = (N-1)/2$. A family of scaling functions can be defined for various choices of azimuthal arc length. An example of $H_1(m)$ and $H_2(m)$ for $\Delta\phi = 30°$ is shown in Figs. A1 and A2.

Evaluating (A4) for any $\Delta\phi$, the scaling functions have unit response at harmonic number $m = \pm 1$. Therefore, a uniform wind can be reproduced exactly. If the radial wind can be decomposed into harmonics having wavenumbers other than $m = \pm 1$, the radial and cross-beam wind estimates will contain these same harmonic variations, with amplitudes determined by (A4).

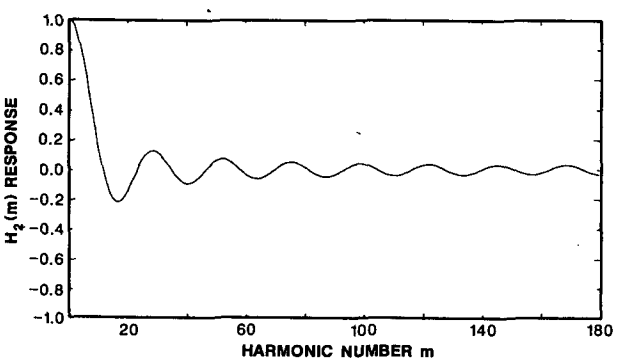

FIG. A2. Response function $H_2(m)$ as a function of harmonic number m for the radial wind estimate. Sector size, $\Delta\phi$, is 30°.

APPENDIX B

Least-Squares Solution of the Linear Wind Model

The functions which project the Cartesian components of a uniform wind are related to functions which project spatial gradients of these components. Thus, the weighting functions become more complicated as higher-order variations in u and v are considered. An analogous expression to (9) for the linear wind model involves inverting a (5 × 5) matrix. Fortunately, the covariance matrix for the regressors ($\boldsymbol{P}_5^{\mathrm{T}}\boldsymbol{P}_5$) can be partitioned into a (2 × 2), a (3 × 3), and two off-diagonal nonsymmetric matrices. The off-diagonal matrices are null natrices because of orthogonality between some regressors.

The general expressions for the least-squares estimates of $\hat{u}_0'$ and $\hat{v}_0'$ are easily shown to be

$$\hat{u}_0' = a_1 \sum v_r(i)\sin[(i-k)\Delta] + a_2 \sum rv_r(i)\sin[2(i-k)\Delta], \quad \text{(B1)}$$

$$\hat{v}_0' = b_0 \sum rv_r(i) + b_1 \sum v_r(i)\cos[(i-k)\Delta] + b_2 \sum rv_r(i)\cos[2(i-k)\Delta], \quad \text{(B2)}$$

where a_1, a_2, b_0, b_1, and b_2 are constants and elements of the inverse covariance matrix of the regressors. The summations are over the range and azimuth extent of the processing area. In a fashion similar to deriving (A4), the scaling functions $H_1(m)$ and $H_2(m)$ for this linear wind model are obtained from the Fourier transform of (B1–B2). In general, the complexity of the analytic expressions for the scaling functions precludes any attempt at deriving them, particularly if the processing area has range extent. It can be shown, however, that the values of both scaling functions are zero for $m = 0$ and $m = \pm 2$, and have unit response for $m = \pm 1$.

The analysis over a circle produces rather simple response functions. For this case, the ($\boldsymbol{P}_5^{\mathrm{T}}\boldsymbol{P}_5$) covariance matrix is diagonal, and it may be shown that (B1) and (B2) become

$$\hat{u}_0' = a_1 \sum v_r(i)\sin[(i-k)\Delta],$$
$$\hat{v}_0' = b_1 \sum v_r(i)\cos[(i-k)\Delta]. \quad \text{(B3)}$$

The constants a_1 and b_1 come from the inverse covariance matrix and are

$$a_1 = \left\{\sum_{i=1}^{N} \sin^2[(i-k)\Delta]\right\}^{-1} \equiv \frac{2}{N},$$
$$b_1 = \left\{\sum_{i=1}^{N} \cos^2[(i-k)\Delta]\right\}^{-1} \equiv \frac{2}{N}. \quad \text{(B4)}$$

Hence, the least-squares estimates are the sine and cosine amplitudes of the fundamental harmonic of v_r over a circle.

REFERENCES

Browning, K. A., and R. Wexler, 1968: The determination of kinematic properties of a wind field using Doppler radar. *J. Appl. Meteor.*, **7**, 105–113.

Doviak, R. J., and M. J. Berger, 1980: Turbulence and waves in the optically clear planetary boundary layer resolved by dual-Doppler radars. *Radio Sci.*, **15**, 297–317.

——, and D. S. Zrnić, 1984: *Doppler Radar and Weather Observations.* Academic Press, 458 pp.

Draper, W. R., and H. Smith, 1981: *Applied Regression Analysis.* John Wiley, 709 pp.

Glover, K. M., A. W. Bishop and W. Lob, 1968: Wind Measurement by dual beam radar. *13th Radar Meteorology Conf. Proc.*, Amer. Meteor. Soc.

Hogg, D. C., M. T. Decker, F. O. Guiraud, K. B. Earnshaw, D. A. Merritt, K. P. Moran, W. B. Sweezy, R. G. Strauch, E. R. Westwater and C. G. Little, 1983: An automatic profiler of the temperature, wind and humidity in the tropopause. *J. Appl. Meteor.*, **22**, 807–831.

Koscielny, A. J., R. J. Doviak and R. M. Rabin, 1982: Statistical considerations in the estimation of divergence from single-Doppler radar and applications to prestorm boundary-layer observations. *J. Appl. Meteor.*, **21**, 197–210.

——, —— and D. S. Zrnić, 1984: An evaluation of the accuracy of some radar wind profiling techniques. *J. Atmos. Oceanic Technol.*, **1**, 309–320.

Lhermitte, R. M., and D. Atlas, 1961: Precipitation motion by pulse Doppler. *Proc. Ninth Weather Radar Conf.*, Boston, Amer. Meteor. Soc., 218–223.

Rabin, R., and D. S. Zrnić, 1980: Subsynoptic-scale vertical wind revealed by dual Doppler-radar and VAD analysis. *J. Atmos. Sci.*, **37**, 644–654.

Smith, S. D., 1986: Sectorized uniform wind algorithm. Report to the NEXRAD Joint System Program Office.

Strauch, R. G., D. A. Merritt, K. P. Moran, K. B. Earnshaw and D. Van de Kamp, 1984: The Colorado wind-profiling network. *J. Atmos. Oceanic Technol.*, **1**, 37–49.

Waldteufel, P., and H. Corbin, 1979: On the analysis of single-Doppler data. *J. Appl. Meteor.*, **18**, 532–542.

Witt, A., and S. D. Smith, 1987: Development and testing of the gust front algorithm. FAA Rep.

Wolfsberg, D. G., 1987: Retrieval of three-dimensional wind and temperature fields from single Doppler radar data. CIMMS Report 84, University of Oklahoma, 91 pp.

Zrnić, D. S., S. D. Smith, A. Witt, R. M. Rabin and M. Sachidananda, 1986: Wind profiling of stormy and quiescent atmospheres with microwave radars. NOAA Tech. Memo. ERL NSSL-98.